Nanoscale

Accepted Manuscript

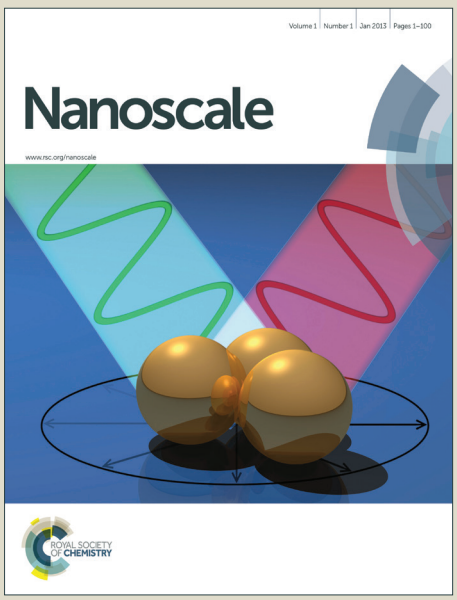

This is an *Accepted Manuscript*, which has been through the Royal Society of Chemistry peer review process and has been accepted for publication.

Accepted Manuscripts are published online shortly after acceptance, before technical editing, formatting and proof reading. Using this free service, authors can make their results available to the community, in citable form, before we publish the edited article. We will replace this *Accepted Manuscript* with the edited and formatted *Advance Article* as soon as it is available.

You can find more information about *Accepted Manuscripts* in the Information for Authors.

Please note that technical editing may introduce minor changes to the text and/or graphics, which may alter content. The journal's standard Terms & Conditions and the Ethical guidelines still apply. In no event shall the Royal Society of Chemistry be held responsible for any errors or omissions in this *Accepted Manuscript* or any consequences arising from the use of any information it contains.

ROYAL SOCIETY OF CHEMISTRY

www.rsc.org/nanoscale

Nanoscale Imaging of Freestanding Nitrogen Doped Single layer Graphene

Ganjigunte R. S. Iyer,*[‡] Jian Wang,[‡] Garth Wells,[‡] Michael P. Bradley[§] and Ferenc Borondics*[‡†]

[‡] *Canadian Light Source, 44 Innovation Boulevard, Saskatoon, SK, S7N 2V3, Canada*

[§] *Dept. of Physics and Engineering Physics, University of Saskatchewan, SK, S7N 5E2, Canada*

ABSTRACT Graphene can be *p*-type or *n*-type doped by introduction of specific species. Doping can modulate the electronic properties of graphene, but opening a sizable-well-tuned bandgap is essential for graphene-based tunable electronic devices. N-doped graphene is widely used for device applications and is mostly achieved by introducing ammonia into the synthesis gas during the chemical vapor deposition (CVD) process. Post synthesis treatment studies to fine-tune the electron hole doping in graphene are limited. In this work realization of N-doping in large area freestanding single layer graphene (LFG) is achieved by post treatment in nitrogen plasma. The changes in the chemical and electronic properties of graphene are followed with Raman microscopy and mapped *via* synchrotron based scanning transmission X-ray microscopy (STXM) at the nanoscale.

Nanoscale Accepted Manuscript

There has been continued interest in graphene and its exotic properties for a broad spectrum of diverse applications ranging from electronic,[1] energy harvesting,[2-4] electrochemical and biosensing.[5, 6] However, the use of intrinsic graphene in most of these applications is limited due to its zero band gap nature and requires sizeable bandgap opening. Tremendous research efforts are directed towards tailoring the electronic properties of graphene by substitutional doping during growth[1, 2, 4, 7-11] or by controlled introduction of heteroatoms *via* chemical[3, 5, 12,13] or physical doping post growth.[10, 14, 15] Nitrogen[1, 8, 14, 16-19] and boron[15, 20] doping of carbon nanomaterials has been a promising route to achieve either *n*- or *p*-type doping by the introduction of electrons or holes. Nonetheless, it is critical to understand the site of inserted dopants in the carbon matrix and its diverse effects on the local electronic structure, highly desirable for tunable electronic devices. Although, there have been considerable efforts to understand the bond types and electronic structure variations in graphene using various characterization methods, they are limited either by the resolution of the technique or the system itself.[17, 18, 21] Most of the studies focused on N-graphene so far involve a supporting system known to modify the electronic structure of the overlying graphene also dramatically affecting device properties and performance.[22]

In this report we address the problems described above: (i) Large area freestanding graphene samples are used to avoid the substrate effect (ii) post growth low energy nitrogen ion implantation in the suspended system for controlled doping and (iii) using high-resolution STXM to map the local electronic structure variations at the nanoscale in the suspended N-graphene. Furthermore, we carried out angle-dependent STXM measurements to understand the effect of N-doping and the preferential orientation of nitrogen in the N.doped LFG (NLFG).

Nanoscale Accepted Manuscript

RESULTS AND DISCUSSION

LFG samples are obtained by etching the supporting copper substrate and transferred on to a TEM grid as described in our previous report.[23] Nitrogen doping of LFG is achieved by low energy nitrogen ion implantation *via* plasma treatment. The samples were treated using an inductively coupled RF plasma source with N_2 flow rate of 20 SCCM, ion density $n_0 = 4\times10^9$ cm^{-3}, electron temperature T_e = 4 eV at 100 W for 2, 5 and 10 minutes (see Supporting Information for details). The bombardment conditions such as the bombardment energy and time are known to affect the level of doping and final bonding configurations.[24-26] Here we focus on the effect of bombardment time on the LFG. In contrast to the previous methods of N-doping by the introduction of NH_3 or other dopant species to the feedstock during CVD graphene growth,[2, 7, 9] post plasma[14, 26] and electrothermal treatments with ammonia,[19] the N-doping of LFG in our case is carried out after the transfer process *i.e.,* on a freestanding sample.

Figure 1a shows the Raman spectra acquired using 532 nm laser excitation for LFG and NLFG samples at 2, 5 and 10 minutes labeled as NLFG-2, NLFG-5 and NLFG-10, respectively. The G and the 2D band seen at 1582 and 2690 cm^{-1} and a negligibly small D band at 1350 cm^{-1} are consistent with the freestanding graphene. The emergence of a prominent D band and shifts in the G and 2D peaks in NLFG relative to the LFG sample are related to nitrogen doping. While there is a monotonous increase in the D band intensity, there is a significant upshift in the G and the 2D bands with the exposure time. It is well known that doping in graphene alters the Fermi surface, resulting in the G and 2D resonances shifts.[27, 28] Notably, initial upshifts in the G and 2D bands observed for the NLFG-2 samples with further upshift in the G-band on longer exposure time as in NLFG-5 and NLFG-10 samples indicate *n*-type doping.[27] Further, increase in the I_D/I_G and I_G/I_{2D} ratio (*inset*, Figure 1b) and FWHM of the G band (Figure 1c) are the consequence of

Nanoscale Accepted Manuscript

n-type doping in graphene. The change in the I_D/I_G ratio with the plasma treatment further corroborates nitrogen inclusion in the NLFG. Interestingly, a small increase in D, D' bands and decrease in the 2D band observed for the N-doped suspended graphene here is in contrast to other techniques, which have shown remarkably stronger D, D' bands along with sharp decrease of 2D band. This indicates that the plasma treatment used in our work is more controllable and milder than those used in other studies.[14, 21]

Nitrogen doping in carbon materials, CNTs in particular, is well established and nitrogen is known to bond in three prominent sites: (i) pyridine-like, (ii) cyanic or pyrolic and (iii) graphite-like sites in the carbon matrix.[17, 18, 24, 25, 29] Each of the boding configuration has great implication on the properties of the doped materials. Although, Raman spectroscopy provides insight on the macroscopic details of N-doping in graphene, it is critical to understand and identify the bonding types along with the changes to the electronic structure of the carbon matrix at the nanoscale. The use of synchrotron radiation at high spatial (30 nm) and energy (0.05 eV) resolution makes STXM a suitable technique to acquire a detailed map of the unoccupied density of states (UDOS) thereby providing a direct image of N speciation and electronic structure at the nanoscale for N-doped graphene. The STXM measurements were carried out at the SM beamline (ID101), CLSI. The measurements were carried out at 90° (sample surface parallel to the E vector of the incident X-ray beam) and 60°(sample tilted by 30°) incident angles.

Figure 2a shows the schematic of possible types of nitrogen sites in the NLFG after N-doping. We identify the pyridine-like, pyrolic or nitrile-like and graphite-like configurations as N1, N2 and N3 respectively. Figure 2b, c show the angle dependent C-K and N-K edge NEXAFS spectra extracted from the respective STXM image stacks. The normal incidence

Nanoscale Accepted Manuscript

reference C-K edge NEXAFS spectrum of the LFG sample shows no π* resonance but a sharp σ* excitonic and broad σ* resonance at 291.6 eV and 292.6 eV, respectively, characteristic of single layer graphene.[17, 18, 21, 22, 30] Ideally for a perfectly flat graphene sample, one should not observe a π* resonance as these orbitals are oriented orthogonal to the basal plane of graphene and to the **E** vector of the in-plane circularly polarized incident X-ray beam. The absence of π* resonance at 285 eV in the LFG indicates the flatness of our freestanding single layer graphene starting material. Also, the absence of the peaks between 287-289 eV and the sharp excitonic feature peak suggests a clean and highly ordered uniform starting material. The NLFG samples show angle dependence as previously observed.[17, 18] In contrast to the LFG, the NLFG samples exhibit a prominent π* resonance at 285 eV and intermediate peaks at 287.5 eV and 288.4 eV in addition to similar σ* features. Moreover, there are no significant disparities in the distinct features from alike samples but for substantial variations in the intensities arising due to the incidence angle. However, there is a distinct pattern in all the discernible spectral features with respect to the bonding configuration and electronic structure upon nitrogen inclusion with increasing bombarding time. Considering the relative intensities of the 1s → π* and 1s → σ* transitions in the NLFG samples at 30° (solid lines), a combination of a stronger π* resonance along with better-defined intermediate peaks at 287.5 eV (isolated $\pi^*_{C=N}$) and 288.4 eV ($\pi^*_{N-C=N}$)[31] and prominent excitonic peak is observed in the NLFG-2 compared to others. This strongly infers that N incorporation is predominantly substitutional or graphitic-N relative to pyridine-like N substitution in the carbon matrix with least structural distortion to the π conjugated graphitic network. Furthermore, for longer bombardment time we observe a substantial increase in the overall intensity of the intermediate features between 287 and 291 eV, however becoming less defined. This is accompanied by a small shift in the π* resonances and

Nanoscale Accepted Manuscript

decrease in the excitonic features. These changes observed at the nanoscale are in consensus with micro Raman measurements, confirming the increase in N functionalities arising from enhanced pyridine-like N substitution, pyrolic-N and dangling C-N due to defect sites.

The effect of N substitution in the carbon network of the NLFG samples is further probed by angle dependent N-K edge NEXAFS spectra obtained by STXM mapping (Figure 2c). Due to smaller X-ray absorption cross-section at the N K-edge and lower concentration, the spectral intensity and signal to noise ratio are both lower than at the C K-edge, which make the difference less prominent. Nevertheless, three spectral features associated to different N sites, N1, N2 and N3 marginally discernible at 398.2, 399.5 and 401.4 eV respectively, represent the π* resonance; while a broad resonance starting at 405 eV to the σ* resonance. The N3 peak is markedly resolved in all the NLFG samples, notably defined in the NLFG-2, indicates predominant graphitic-N, in agreement with the corresponding C-K edge spectrum. In addition, emergence of N1 in both the NLFG-5 and NLFG-10 samples indicates distinct N-C species. At increased bombardment time, the NLFG, shows a weaker π* and a relatively stronger, broader and energy-upshifted σ* resonance, leading to enhanced C-N contributions arising mostly from N1 and N2 dopants. This is in good agreement with the enhanced D band intensity observed in the Raman spectra. DFT calculations for NSLG have indicated that graphitic-N or the substitutional-N *n*-dopes the graphene, while the pyridine-like or nitrile-like, due to vacancies, defects and edges introduces *p*-doping.[17] The significant graphite-like sites as seen from both C and N-K edge NEXAFS spectra and upshifts of the Raman G band for the NLFG coupled with the emergence of the N1, N2 features along with enhanced D band intensity and downshift in G band frequency in the NLFG-5 sample, indicate *n*- and *p*-doping respectively. This is further corroborated by the normal incident O-K edge spectra as seen in Figure 3. The O-K edge spectra exhibit two main

Nanoscale Accepted Manuscript

features, resonance at 534 eV and 540 eV corresponding to π*(C=O) and σ*(C-O).[24] The negligibly smaller intensities of the spectra for a smaller bombardment time are consistent with the C and N-K edge spectra indicating significant C-N related contributions. At higher bombardment time, *i.e.*, NLFG-10 the intensity and the area of the peak are relatively enhanced compared to NLFG-2 and NLFG-5. The ion bombardment introduces nitrogen related vacancies edge defects and increased amount of unsaturated carbon at these sites, which act as the sites of oxygen uptake in the LFG. These changes in the NLFG-10 are in agreement with the increased nitrile and pyridine-like sites and enhanced D band intensity as observed from both the C and N-K edge NEXAFS spectra and Raman studies.

Chemical mapping of the same regions of the NLFG samples were performed at the C and N-K edges to image the C-N configurations in the carbon matrix. The mapping of NLFG-5 is plotted in linearly scaled rainbow color scheme for the C-K and N-K edge as shown in Figure 4(a-c) and 4(d-f) respectively. The average optical density (OD) (Figure 3a), measure of the thickness of the material, shows the film to be fairly uniform in most of the regions. The contribution of the $\pi^*_{C=C}$ was mapped by subtracting the pre-edge and found to be uniformly distributed in the flat regions and understandably increasing at the wrinkled or folded regions (Figure 4b). The π^*_{C-N} mapped between 287-288 eV (Figure 4c) shows a more even distribution of nitrogen than $\pi^*_{C=C}$ due to uniform implantation of nitrogen on the sample surface regardless the wrinkled or folded regions. To further substantiate bonding types and the homogeneity effect of N-incorporation chemical imaging of the N-K edge was performed. Figure 3d shows the average OD of the N-K edge smaller compared to the C-K edge, which can be attributed to the X-ray absorption cross-section difference between nitrogen and carbon, the former being smaller than the later. The N1s → $\pi^*_{C=N}$ transitions mapped between 398-402 eV as seen in Figure 3e

Nanoscale Accepted Manuscript

shows nitrogen to be highly concentrated as substitutional-N in the flat regions corroborating the planar N-C. Further, N1s→ σ* transitions depicts similar chemical pattern with the more flatness/crystallinity the higher σ* intensity. The areas above the center empty region in Figure 3f show stronger σ* intensity than other regions, suggesting better flatness and quality of nitrogen doped graphene.

The spectroscopic details from STXM NEXAFS and Raman scattering corroborates with the reported DFT calculations for nitrogen-doped graphene. It must be stressed here that the doping observed in the NLFG is solely due the nitrogen attached to the carbon matrix as a result of nitrogen ion bombardment removing any ambiguity of the influence of the underlying substrate. This is of great importance as most of the reports on N-doping of graphene thus far are carried out on supported systems.[14, 17-19, 26] The interfacial interaction at graphene-metal[23, 32] and graphene-dielectric interface is known to hybridise the electronic points at K and K' resulting in bandgap opening.[33, 34] Additionally in the supported system, it is highly probable for the nitrogen to either attach to the substrate or the substrate-sample interface along with graphene, which can be ruled out in our freestanding samples.

CONCLUSIONS

In summary, we present N-doping studies of large area freestanding single layer graphene *via* low energy nitrogen ion implantation carried out using RF plasma. Bond types and C-N configuration are mapped at the nanoscale by STXM and corroborated by Raman scattering. The C and N-K edge STXM mapping confirms nitrogen is bonded to the single layer of carbon sheet as mostly the graphitic-N and substitutional-N. The small increase in the D-band intensity from the Raman studies for higher bombardment time accompanied by negligibly small amounts of oxygen and unsaturated carbon as seen from the O and C-K edge, validates the effect of nitrogen

Nanoscale Accepted Manuscript

implantation to be milder as compared to other methods implemented for the nitrogen doping of SLG. Importantly, the nitrogen doping study of substrate-free graphene eradicates the profound effect of interfacial interactions on the electronic structure of the atomic layer and confirms the nitrogen bonding in the carbon matrix. Our work demonstrates a clean transfer process and a mild plasma treatment: a preparation route with precise band-gap control for optoelectronic applications.

MATERIALS AND METHODS

Materials:

(i) Sample Preparation: The Single Layer Graphene (SLG) synthesized on copper (Cu) substrates via Chemical Vapor Deposition (CVD) technique, purchased from Graphene SuperMarket are used in this study. The underlying Cu substrate is etched off using 0.1 M ammonium per sulphate solution followed by multiple rinsing in DI water to prepare Large Area Freestanding SLG (LFG) samples. These LFG samples are then carefully scooped from the DI water to be transferred onto Au coated perforated TEM grid(s) with 40 µm x 40 µm perforation size (3 mm, 400 mesh company SPI, 433HG-CF). The holey carbon supported TEM grids are particularly avoided for any ambiguity arising due to the carbon support in the analysis of LFG.

(ii) Nitrogen Doped Freestanding Graphene (NLFG): To fabricate nitrogen doped LFG (N-LFG), nitrogen ion bombardment was carried using an inductively coupled plasma (ICP) generated in a 20 L stainless steel vacuum chamber ICPII-600 (base pressure < 10^{-6} Torr) fed by N_2 feedstock gas. The transferred freestanding graphene *i.e.*, LFG samples were treated in nitrogen plasma using 100 W RF power for 2, 5 and 10 min under 20 sccm nitrogen flow rate

Nanoscale Accepted Manuscript

respectively. Nitrogen doping is carried in the freestanding graphene to avoid the ambiguity of nitrogen attachment either in the graphene-substrate interface or the underlying substrate.

II Materials Characterisation:

(i) Raman Spectroscopy: Renishaw 2000 system at the Mid-IR beamline of CLSI Raman spectrometer was used to record the Raman spectra of the LFG and NLFG samples. The measurements were carried using a 532 nm excitation and 50X objective and 1800 line/mm grating. Short accumulation times and low power (~2.5 mW) were used to avoid localised heating from the laser.

(ii) Scanning Transmission X-ray Microscopy (STXM): The STXM measurements were carried out at the Spectromicroscopy (SM) 10ID-1 beamline at CLSI, a 2.9 GeV third generation synchrotron facility. The SM beamline is equipped with a 25 nm outermost Fresnel's zone plate providing 30 nm spatial resolution and Elliptically Polarised Undulator (EPU) source. A 250 line/mm and 500 line/mm, plane-grating monochromator (PGM) was used for C, N K-edge and O-K edge measurements respectively. The incident photon flux (I_o) is focused into a spot by the Fresnel's zone plate while the Order Sorting Aperture (OSA) allows only the 1st order filtering the rest. The count rate of the I_o was tuned to 20 MHz at 320 eV with the 35/35 mm dispersive/non-dispersive exit slits. The sample was raster-scanned with synchronized detection of transmitted X-rays to generate image sequence (stacks) over a range of photon energies specific to the element of interest such as C, N_2 and O_2 respectively. In this study two sample orientations were used: firstly, the incident photon beam is normal to the sample surface such that the electric polarization vector of the X-Ray beam lies parallel to the sample surface *i.e.*, the basal plane of the graphene sheet. Secondly, the sample is titled by 30 degree *i.e.*, 60 degrees

Nanoscale Accepted Manuscript

with respect to the incident X-ray beam and the sample normal. The STXM data was analysed using aXis2000 (available at http://unicorn.mcmaster.ca/aXis2000.html). The collected image sequence from the Region of Interest (ROI) were first aligned, and then converted to optical density (OD) by using the incident flux (I_o) spectrum collected from an empty region preferably hole adjoint to the ROI during the measurement. The colour composite maps were generated from the average OD image by combining individual component maps using PC analysis and the corresponding C, N and O-K edge NEXAFS spectra were derived from the same regions.

AUTHOR INFORMATION

***Corresponding Author**

Email: Swathi.Iyer@lightsource.ca, Ferenc.Borondics@synchrotron-soleil.fr

Present Addresses

† Soleil Synchrotron
L'Orme des Merisiers, Saint-Aubin BP 48
91192 Gif-sur-Yvette Cedex, France

Author Contributions

All authors have given approval to the final version of the manuscript.

Acknwoledgements

Research described in this paper was performed at the Mid-IR, SM and SyLMAND beamlines of the Canadian Light Source, which is supported by the Natural Sciences and Engineering

Nanoscale Accepted Manuscript

Research Council of Canada, the National Research Council Canada, the Canadian Institutes of Health Research, the Province of Saskatchewan, Western Economic Diversification Canada, and the University of Saskatchewan.

NOTES AND REFERENCES

1. D. Wei, Y. Liu, Y. Wang, H. Zhang, L. Huang and G. Yu, *Nano Lett.*, 2009, **9**, 1752-1758.
2. A. L. M. Reddy, A. Srivastava, S. R. Gowda, H. Gullapalli, M. Dubey and P. M. Ajayan, *ACS Nano*, 2010, **4**, 6337-6342.
3. H. M. Jeong, J. W. Lee, W. H. Shin, Y. J. Choi, H. J. Shin, J. K. Kang and J. W. Choi, *Nano Lett.*, 2011, **11**, 2472-2477.
4. L. Qu, Y. Liu, J.-B. Baek and L. Dai, *ACS Nano*, 2010, **4**, 1321-1326.
5. Y. Wang, Y. Shao, D. W. Matson, J. Li and Y. Lin, *ACS Nano*, 2010, **4**, 1790-1798.
6. C.-H. Lu, H.-H. Yang, C.-L. Zhu, X. Chen and G.-N. Chen, *Angew. Chem. Int. Ed.*, 2009, **48**, 4785-4787.
7. Z. Jin, J. Yao, C. Kittrell and J. M. Tour, *ACS Nano*, 2011, **5**, 4112-4117.
8. H. Wang, T. Maiyalagan and X. Wang, *ACS Catal.*, 2012, **2**, 781-794.
9. Y. Xue, B. Wu, L. Jiang, Y. Guo, L. Huang, J. Chen, J. Tan, D. Geng, B. Luo, W. Hu, G. Yu and Y. Liu, *J. Am. Chem. Soc.*, 2012, **134**, 11060-11063.
10. C. Zhang, L. Fu, N. Liu, M. Liu, Y. Wang and Z. Liu, *Adv. Mater.*, 2011, **23**, 1020-1024.
11. B. J. Schultz, R. V. Dennis, V. Lee and S. Banerjee, *Nanoscale*, 2014, **6**, 3444-3466.
12. L. Feng, L. Yang, Z. Huang, J. Luo, M. Li, D. Wang and Y. Chen, *Sci. Rep.*, 2013, **3**.
13. Y. Kim, J. Park, J. Kang, J. M. Yoo, K. Choi, E. S. Kim, J.-B. Choi, C. Hwang, K. S. Novoselov and B. H. Hong, *Nanoscale*, 2014, **6**, 9545-9549.
14. Y.-C. Lin, C.-Y. Lin and P.-W. Chiu, *App. Phys. Lett.*, 2010, **96**, -.
15. L. S. Panchakarla, K. S. Subrahmanyam, S. K. Saha, A. Govindaraj, H. R. Krishnamurthy, U. V. Waghmare and C. N. R. Rao, *Adv. Mater.*, 2009, **21**, 4726-4730.
16. B. Guo, Q. Liu, E. Chen, H. Zhu, L. Fang and J. R. Gong, *Nano Lett.*, 2010, **10**, 4975-4980.
17. T. Schiros, D. Nordlund, L. Pálová, D. Prezzi, L. Zhao, K. S. Kim, U. Wurstbauer, C. Gutiérrez, D. Delongchamp, C. Jaye, D. Fischer, H. Ogasawara, L. G. M. Pettersson, D. R. Reichman, P. Kim, M. S. Hybertsen and A. N. Pasupathy, *Nano Lett.*, 2012, **12**, 4025-4031.
18. D. Usachov, O. Vilkov, A. Grüneis, D. Haberer, A. Fedorov, V. K. Adamchuk, A. B. Preobrajenski, P. Dudin, A. Barinov, M. Oehzelt, C. Laubschat and D. V. Vyalikh, *Nano Lett.*, 2011, **11**, 5401-5407.
19. X. Wang, X. Li, L. Zhang, Y. Yoon, P. K. Weber, H. Wang, J. Guo and H. Dai, *Science*, 2009, **324**, 768-771.
20. L. Zhao, M. Levendorf, S. Goncher, T. Schiros, L. Pálová, A. Zabet-Khosousi, K. T. Rim, C. Gutiérrez, D. Nordlund, C. Jaye, M. Hybertsen, D. Reichman, G. W. Flynn, J. Park and A. N. Pasupathy, *Nano Lett.*, 2013, **13**, 4659-4665.
21. L. Zhao, R. He, K. T. Rim, T. Schiros, K. S. Kim, H. Zhou, C. Gutiérrez, S. P. Chockalingam, C. J. Arguello, L. Pálová, D. Nordlund, M. S. Hybertsen, D. R.

Nanoscale Accepted Manuscript

Reichman, T. F. Heinz, P. Kim, A. Pinczuk, G. W. Flynn and A. N. Pasupathy, *Science*, 2011, **333**, 999-1003.
22. V. Lee, C. Park, C. Jaye, D. A. Fischer, Q. Yu, W. Wu, Z. Liu, J. Bao, S.-S. Pei, C. Smith, P. Lysaght and S. Banerjee, *J. Phys. Chem. Lett.*, 2010, **1**, 1247-1253.
23. G. R. S. Iyer, J. Wang, G. Wells, S. Guruvenket, S. Payne, M. Bradley and F. Borondics, *ACS Nano*, 2014, **8**, 6353-6362.
24. G. Abbas, P. Papakonstantinou, G. R. S. Iyer, I. W. Kirkman and L. C. Chen, *Phys.Rev. B*, 2007, **75**, 195429.
25. G. R. S. Iyer and P. D. Maguire, *J. Mater. Chem.*, 2011, **21**, 16162-16169.
26. W. Zhao, O. Höfert, K. Gotterbarm, J. F. Zhu, C. Papp and H. P. Steinrück, *J. Phys.Chem. C*, 2012, **116**, 5062-5066.
27. DasA, PisanaS, ChakrabortyB, PiscanecS, S. K. Saha, U. V. Waghmare, K. S. Novoselov, H. R. Krishnamurthy, A. K. Geim, A. C. Ferrari and A. K. Sood, *Nat. Nanotechnol.*, 2008, **3**, 210-215.
28. S. Pisana, M. Lazzeri, C. Casiraghi, K. S. Novoselov, A. K. Geim, A. C. Ferrari and F. Mauri, *Nat. Mater.*, 2007, **6**, 198-201.
29. J. Zhou, J. Wang, H. Liu, M. N. Banis, X. Sun and T.-K. Sham, *J. Phys. Chem. Lett.*, 2010, **1**, 1709-1713.
30. B. J. Schultz, C. J. Patridge, V. Lee, C. Jaye, P. S. Lysaght, C. Smith, J. Barnett, D. A. Fischer, D. Prendergast and S. Banerjee, *Nat. Commun.*, 2011, **2**, 372.
31. A. Fujimori, N. Sato, K. Kanai, Y. Ouchi and K. Seki, *Langmuir*, 2008, **25**, 1112-1121.
32. J. Lee, K. S. Novoselov and H. S. Shin, *ACS Nano*, 2010, **5**, 608-612.
33. S. Y. Zhou, G. H. Gweon, A. V. Fedorov, P. N. First, W. A. de Heer, D. H. Lee, F. Guinea, A. H. Castro Neto and A. Lanzara, *Nat. Mater.*, 2007, **6**, 770-775.
34. G. Giovannetti, P. A. Khomyakov, G. Brocks, P. J. Kelly and J. van den Brink, *Phys. Rev. B*, 2007, **76**, 073103.

Nanoscale Accepted Manuscript

FIGURES

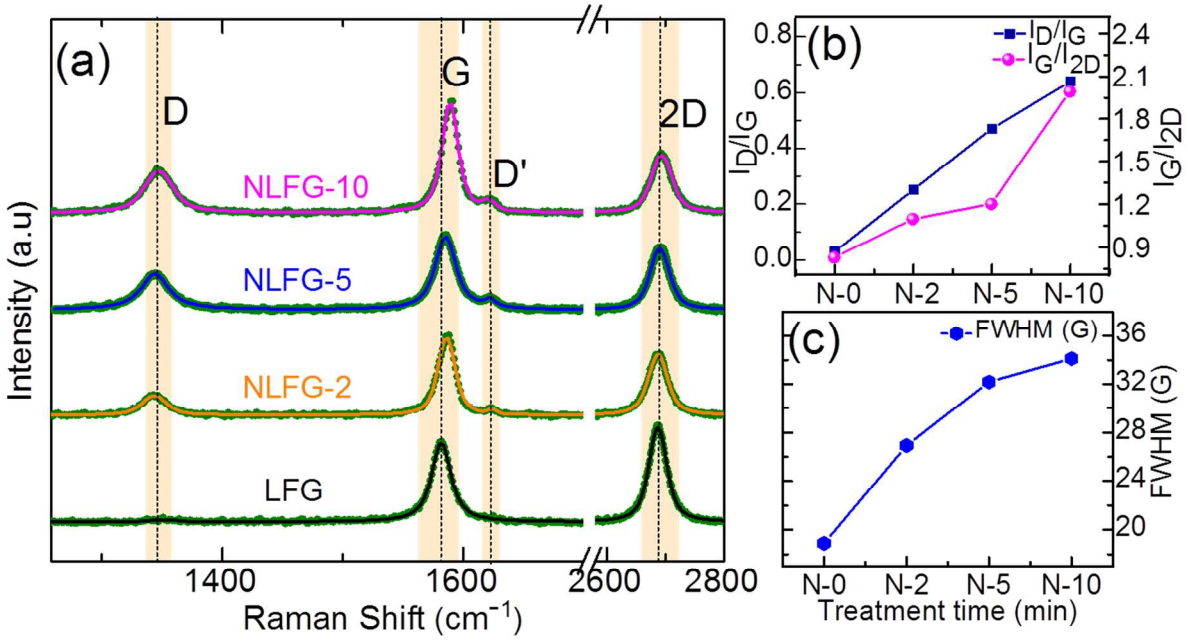

Figure 1. (a) Overlay of LFG and NLFG samples (inset) (b) I_D/I_G and I_G/I_{2D} and (c) fullwidth half maxima of nitrogen treated LFG at various time.

Nanoscale Accepted Manuscript

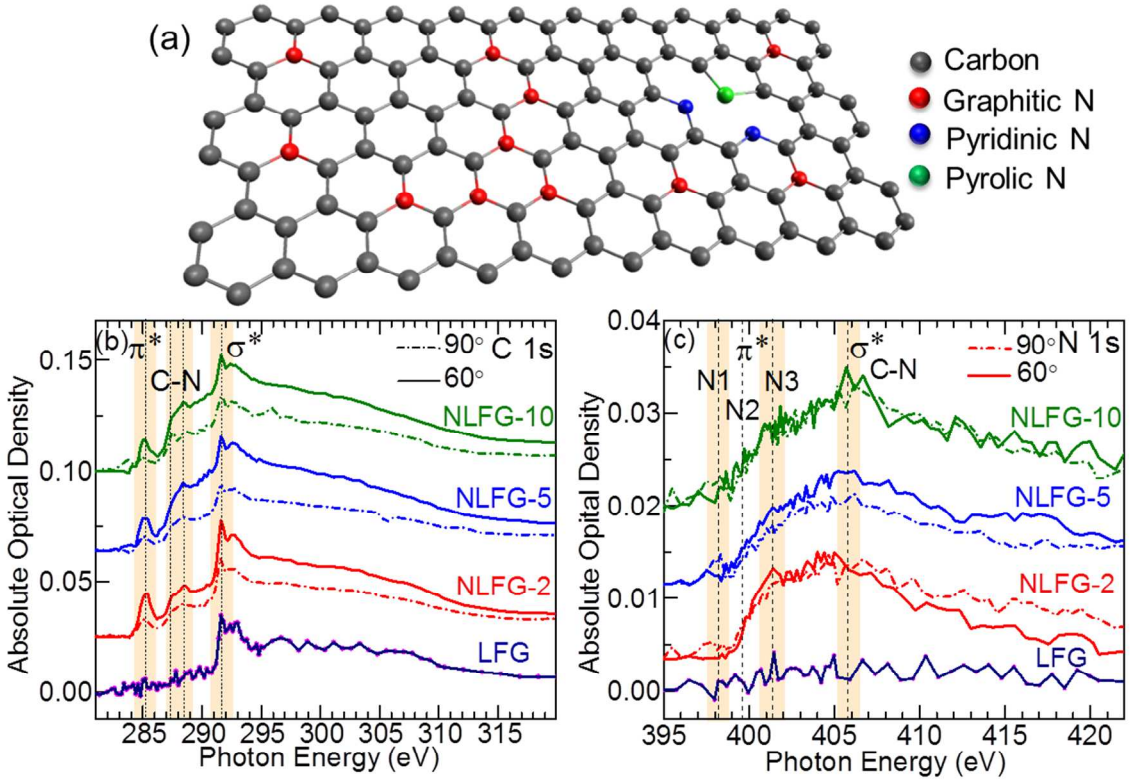

Figure 2. (a) Schematic of the orientations of the basal plane w.r.t the electromagnetic field vector (E) of the incident X-ray beam (hν) and the most probable sites of N attachment in the NLFG sample after N-treatment. The spatially resolved average NEXAFS spectra extracted from the different angle dependent mapping measurements of (b) C-K edge, 280-320 eV and (c) N-K edge, 385-420 eV.

Nanoscale Accepted Manuscript

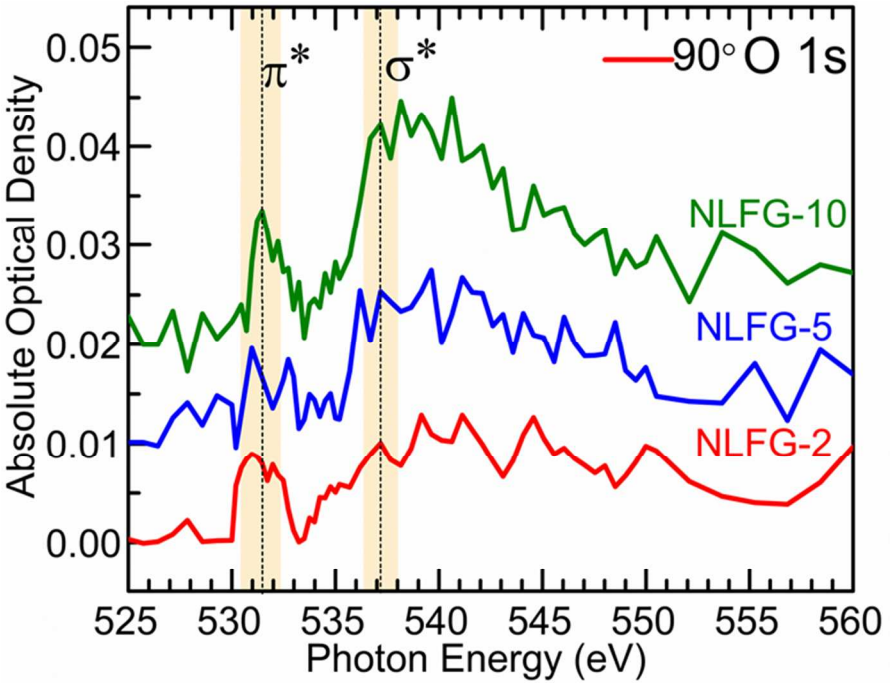

Figure 3. The spatially resolved average O-K edge NEXAFS spectra extracted from the normal incident STXM mapping measurement between 525-560 eV energy range.

Nanoscale Accepted Manuscript

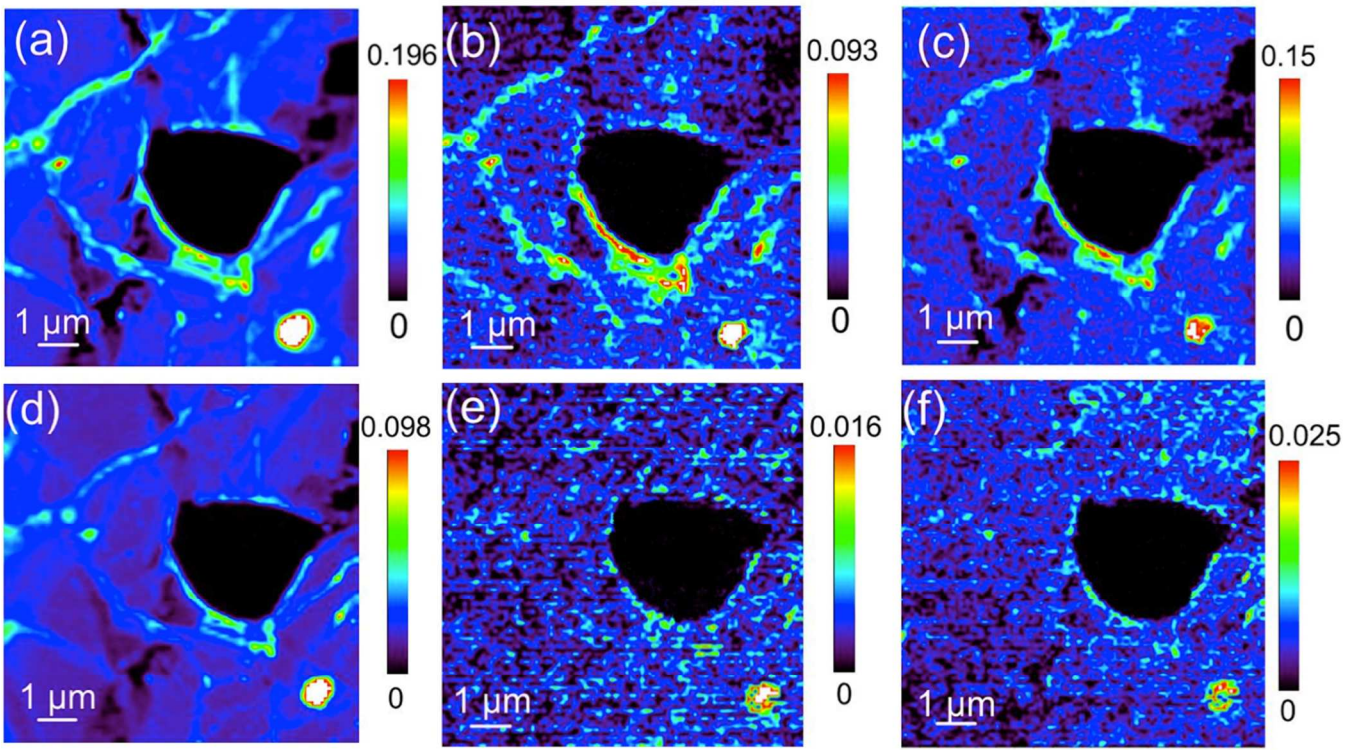

Figure 4. (Top panel) (a) Average OD of the C K edge between 280-320 eV (b) π* (C=C), 284.5-285.5 eV mapping and (c) π* (C-N) between 287-288 eV. (Bottom panel) (d) Average OD of the N K edge between 380-420 eV (e) The N π* (graphitic), 398-402 eV mapping and (f) σ* (C-N) between 406-415 eV for the NLFG-2 at 30º respectively.

Nanoscale Accepted Manuscript

Table of Contents Graphic.

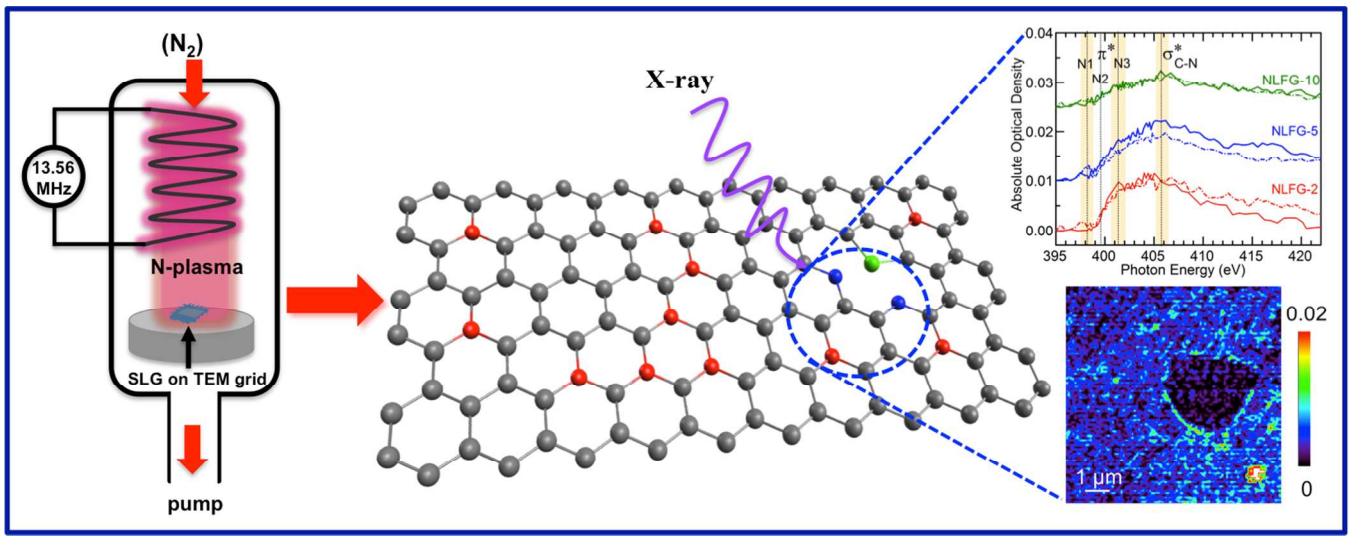

Nanoscale Accepted Manuscript